Laser-driven three-stage heavy-ion acceleration from relativistic laser-plasma interaction

H. Y. Wang,[1,2] C. Lin,[1,*] B. Liu,[1] Z. M. Sheng,[3] H. Y. Lu,[1] W. J. Ma,[4,5] J. H. Bin,[4,5] J. Schreiber,[4,5] X. T. He,[1] J. E. Chen,[1] M. Zepf,[2] and X. Q. Yan[1,†]

[1]*State Key Laboratory of Nuclear Physics and Technology, and Key Lab of High Energy Density Physics Simulation, CAPT, Peking University, Beijing 100871, China*

[2]*Helmholtz Institute Jena, Fröbelstieg 3, 07743 Jena, Germany*

[3]*Key Laboratory for Laser Plasmas (MoE) and Department of Physics and Astronomy, Shanghai Jiao Tong University, Shanghai 200240, China*

[4]*Max-Planck-Institut für Quantenoptik, D-85748 Garching, Germany*

[5]*Fakultät für Physik, LMU München, D-85748 Garching, Germany*

(Received 7 August 2013; published 23 January 2014)

A three-stage heavy ion acceleration scheme for generation of high-energy quasimonoenergetic heavy ion beams is investigated using two-dimensional particle-in-cell simulation and analytical modeling. The scheme is based on the interaction of an intense linearly polarized laser pulse with a compound two-layer target (a front heavy ion layer + a second light ion layer). We identify that, under appropriate conditions, the heavy ions preaccelerated by a two-stage acceleration process in the front layer can be injected into the light ion shock wave in the second layer for a further third-stage acceleration. These injected heavy ions are not influenced by the screening effect from the light ions, and an isolated high-energy heavy ion beam with relatively low-energy spread is thus formed. Two-dimensional particle-in-cell simulations show that ∼100 MeV/u quasimonoenergetic Fe^{24+} beams can be obtained by linearly polarized laser pulses at intensities of 1.1×10^{21} W/cm^2.

DOI: 10.1103/PhysRevE.89.013107 PACS number(s): 52.38.Kd, 41.75.Jv, 52.35.Mw, 52.59.−f

I. INTRODUCTION

During the past decade, the generation of energetic ion beams from ultrahigh-intensity lasers has attracted much interest due to its many applications [1,2]. Several promising ion acceleration schemes were proposed, such as target normal sheath acceleration (TNSA) [3], collisionless electrostatic shock acceleration [4,5], radiation pressure acceleration [6], and breakout afterburner acceleration [7]. However, most of these schemes are based on protons or light ions, while generation of high-energy heavy ions is still difficult due to a certain physical limit. In experiments for a typical metal target contaminated with lighter ions (hydrogen, carbon, and oxygen), lighter ions are dominantly accelerated, thereby screening the acceleration potential for heavier ions. Resistive heating or laser ablation can reduce the target-backside contaminants, allowing generation of heavy ions with energies up to multi-MeV/u [8–10]. Recently in theory a compound target was proposed to generate quasimonoenergetic Fe^{24+} beams with energy up to 36 MeV/u at laser intensity of 10^{22} W/cm^2 [11]. Such laser-driven heavy ion sources may enable significant advances in the development of compact heavy ion accelerators [12], heavy ion-driven inertial fusion [13], heavy-ion tumor therapy [14], generation of high-energy-density states in matter [15], and frontier study of quark-gluon plasma by heavy ion collisions [16].

In this paper, we propose a new scheme, named three-stage heavy ion acceleration, to produce high-energy (∼100 MeV/u), high-current (∼MA), and quasimonoenergetic (energy spread of 10%–20%) heavy ion beams at laser intensity of 10^{21} W/cm^2. The scheme is based on the interaction of a linearly polarized (LP) laser pulse with a compound target consisting of a front heavy ion layer attached behind with a second light ion layer. It makes use of three different acceleration mechanisms for three consecutive stages: the first piston-acceleration stage at the heavy ion layer front surface, the second sheath-acceleration stage at the internal interface, and the third shock-acceleration stage in the light ion layer. We identify that, under appropriate conditions, heavy ions preaccelerated by a two-stage acceleration in the front layer can catch up with and be injected in the light ion shock-wave for a further third-stage acceleration, overcoming the screening effect from the lighter ions. That means that these injected heavy ions can be accelerated to much higher energies than screened ions. In this way an isolated high-energy heavy ion beam with relatively low-energy spread is formed. The injection condition has been analytically derived and verified by two-dimensional (2D) particle-in-cell (PIC) simulations. It is shown that a ∼100 MeV/u quasimonoenergetic Fe^{24+} ion beam with energy spread of 16% and ion current of 0.6 MA can be obtained by linearly polarized laser pulses at intensities of 10^{21} W/cm^2.

Compound or multilayer targets have been used earlier for ion acceleration [10,17]. But the heavy ions were mainly used as a heavy background to improve the quality of light ion beams. In contrast, here we propose to use a two-layer target in order to produce high-quality heavy ion beams. Schematic figures of the three stage heavy ion acceleration are depicted in Fig. 1. The target consists of a front heavy ion layer followed by a low-density light ion layer with an exponentially decaying density profile. In our simulations, the front layer is a Fe layer ($Z_1 = 24, A_1 = 56$) with electron density n_{e1} and thickness D (Fe^{24+} ions are produced through field ionization at laser intensity $>10^{20}$ W/cm^2 [11,18]), while the second layer is a C layer ($Z_2 = 6, A_2 = 12$) exponentially decreasing from an electron density n_{e2} with a scale length L. Such a second light ion layer may be naturally realized by laser ablation with a

*lincheng0821@pku.edu.cn
†x.yan@pku.edu.cn

 ©2014 American Physical Society

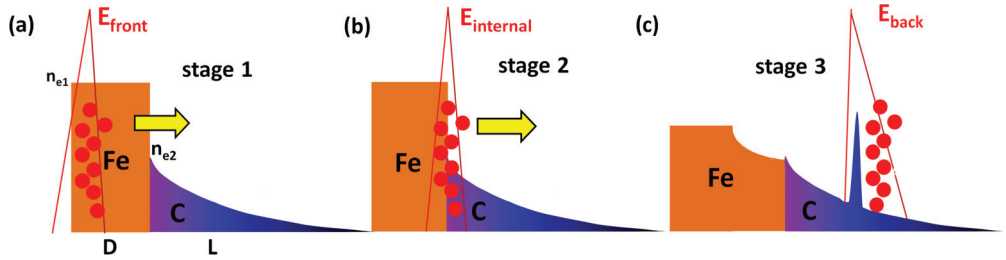

FIG. 1. (Color online) Schematic figures of the three-stage acceleration. (a)–(c) Electrostatic fields E_{front}, E_{internal}, and E_{back} for the corresponding first piston-acceleration stage, second sheath-acceleration stage, and third shock-acceleration stage, respectively.

low-intensity prepulse irradiating on the rear target surface, and the scale length L can be controlled by adjusting the delay between the prepulse and the main pulse [19].

II. THEORY

The process of producing high-energy Fe^{24+} ion beams comprises three consecutive stages. The first stage starts at time t_1 when the laser hits the front Fe layer surface. There the radiation pressure pushes electrons into the target, inducing a charge separation field E_{front}, which accelerates ions in a piston-like manner, as shown in Fig. 1(a). The piston velocity can be obtained from the momentum balance as [20,21]

$$v_{\text{piston}} = a_0 c \left(\frac{Z_1}{A_1} \frac{n_c}{n_{e1}} \frac{m_e}{m_p} \right)^{1/2}, \tag{1}$$

where m_e and m_p are electron mass and proton mass, respectively, $a_0 = 0.85(I_0\lambda^2/10^{18}\ \text{Wcm}^{-2}\ \mu\text{m}^2)^{1/2}$ is the normalized laser amplitude, and $n_c = m_e\omega^2/e^2$ is the critical density. The Fe ions at the front side of the foil can be continuously picked up and reflected by the piston to maximum velocity $v_{\text{Fe},1} \simeq 2v_{\text{piston}}$.

At the same time, the plasma is strongly heated by the $j \times B$ heating effect, as there is the oscillating term for a LP laser pulse. The hot electrons pass through the Fe layer, generating a sheath field E_{internal} at the internal interface of the two layers. The second acceleration stage then sets in at $t_2 = t_1 + D/v_{\text{Fe},1}$ when the Fe ions initially reflected by the piston reach the interface, as shown in Fig. 1(b). E_{internal} can be estimated as $E_{\text{internal}} \sim T_h/e\lambda_D e^{-z/\lambda_D}$ [22], where λ_D is the Debye length of the hot electron $\lambda_D = \sqrt{T_h/4\pi e^2 n_h}$, and T_h and n_h are the hot electron temperature and density, respectively. z is the laser propagation direction, and $z = 0$ is the field peak position.

Due to their larger charge-to-mass ratio, C ions are preferentially accelerated by E_{internal}, just like in Refs. [3]. Since they experience a higher E_{internal}, C ions from the high-density region will move faster than those from low-density region. This results in the formation of a density peak and a comoving electrostatic field E_{back} there, as seen in Fig. 1(c). This process can be interpreted as formation of a C ion shock wave, similar to what has been observed in the Coulomb explosion of nonuniform ion nanoclusters [23]. If the Fe ions preaccelerated by the first two stages gain enough kinetic energy, they can catch up with and be injected into the C ion shock wave at time t_3. These ions are then captured by the shock wave and further accelerated by E_{back}, overcoming the screening effect. This will be referred to as the third-stage of acceleration, as shown in Fig. 1(c). In this way the injected Fe ions are separated with those screened Fe ions, and an isolated Fe ion bunch is formed with a relatively low-energy spread.

The key point for efficient three-stage Fe ion acceleration is that the Fe ions preaccelerated in the first two stages can be injected in the C ion shock wave. If we assume that the averaged electrostatic field experienced by ions at the rear side of the Fe layer is almost a constant before time t_3, $E_{\text{avg}} \sim \int_0^{\lambda_D} E_{\text{internal}}\, dz/\lambda_D = (1 - e^{-1})T_h/e\lambda_D$, the C ion shock velocity at time t is given by $v_{C,t} = \frac{Z_2}{A_2}\frac{m_e}{m_p}(t - t_1)E_{\text{avg}}$, while the maximum Fe ion velocity at time t is $v_{\text{Fe},t} = v_{\text{Fe},1} + \frac{Z_1}{A_1}\frac{m_e}{m_p}(t - t_2)E_{\text{avg}}$. The condition for Fe ion injection is that Fe ions from the front surface can catch up with the C ion shock front at time t:

$$\int_{t1}^{t} v_{c,t}\, dt \leqslant \int_{t2}^{t} v_{Fe,t}\, dt. \tag{2}$$

For simplicity we write the ratio of charge-to-mass ratios of heavy ions to light ions as $f = Z_1A_2/Z_2A_1$ $(0 < f < 1)$ and the acceleration of the C ion shock wave as $a_2 = \frac{Z_2}{A_2}\frac{m_e}{m_p}E_{\text{avg}}$; then Eq. (2) requires

$$D < \frac{v_{Fe,1}^2}{(1 + \sqrt{1 - f})a_2}, \tag{3}$$

and the injection time t_3 is obtained when the equality holds:

$$t_3 = t_1 + D/v_{\text{Fe},1} + \frac{v_{\text{Fe},1} - a_2 D/v_{\text{Fe},1} - \sqrt{v_{\text{Fe},1}^2 + f a_2^2 D^2/v_{\text{Fe},1}^2 - 2a_2 D}}{a_2(1 - f)}. \tag{4}$$

It is known that large plasma gradients $(L > \lambda_D)$ at the rear surface of foil will hamper ion acceleration due to the reduced accelerating electric field [24]. Here we set the scale length of the second layer $L \sim \lambda_D$, so that E_{internal} is not

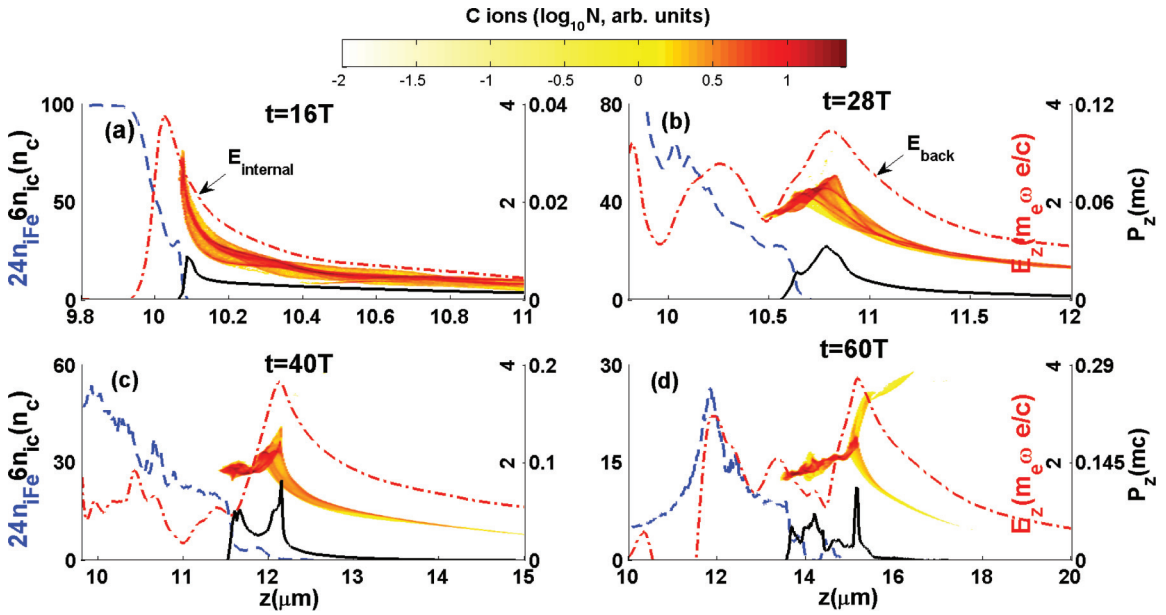

FIG. 2. (Color online) Time evolution for the formation of C ion shock at (a) $t = 16T$, (b) $t = 28T$, (c) $t = 40T$, and (d) $t = 60T$. C ion phase space and on axis longitudinal profiles of Fe ion density $24n_{iFe}$ (blue dashed), C ion density $6n_{ic}$ (solid black), and longitudinal field E_z (dotted red dashed).

significantly affected by the second layer [25]. Then if we estimate $T_h \simeq 0.8a_0$ for $a_0 \gg 1$ [4] and $\lambda_D \sim 1\ \mu$m [26], the injection condition for Eq. (3) can then be revised as

$$D\,(\mu\text{m}) < 5\frac{e}{e-1}\left(\frac{a_0 n_c}{n_{e1}}\right)\frac{f}{1+\sqrt{1-f}}. \tag{5}$$

This means that the Fe layer should be thin enough to satisfy injection condition. On the other hand, if the Fe layer is too thin, the effect of relativistically induced slab transparency (RIST) takes place [28], and the transmitted laser pulse will destroy the C ion shock wave structure. The threshold for RIST of short laser pulse can be estimated as [28] $D \approx \frac{a_0}{\pi n_{e1}}$. For relatively long laser pulse (laser duration τ of hundreds fs), the foil may become transparent due to expansion of the foil. In order to reduce the effect of RIST, it is required that $D \gg \frac{a_0}{\pi n_{e1}}$. Thus the condition for efficient three-stage ion Fe acceleration is

$$\frac{a_0}{\pi n_{e1}} \ll D\,(\mu\text{m}) < 5\frac{e}{e-1}\left(\frac{a_0 n_c}{n_{e1}}\right)\frac{f}{1+\sqrt{1-f}}. \tag{6}$$

It is worth noting that monoenergetic proton acceleration by shock waves has also been examined in experiments by Haberberger *et al.* [5] and theorical studies by Fiuza *et al.* [27]. But their model relies explicitly upon a long scale length ($L \gg \lambda_D$) exponentially decaying plasma profile at the rear side to decrease the amplitude of TNSA fields and is not applicable to the light ion shock wave structure we find in our simulation results.

III. SIMULATION RESULTS

In order to verify the three-stage heavy ion acceleration scheme discussed above, 2D PIC simulations are run with the KLAP2D code [29]. The simulation space (80 μm × 40 μm) is composed of 8000 × 1600 cells along the z and y directions. We choose a LP laser pulse with $I_0 = 1.1 \times 10^{21}$ W/cm^2 (corresponding to $a_0 = 28$), $\lambda = 1.0\ \mu$m, and Gaussian intensity distribution $\exp[-(r/r_0)^2]$ propagating along the z axis, where $r_0 = 2\ \mu$m is the spot radius. The laser pulse has a trapezoidal temporal profile of duration $80T$ ($T = 2\pi/\omega$), consisting of a plateau of $78T$ and rising and falling times of $1T$ each. The front Fe_{56}^{24+} layer with electron density $n_{e10} = 100n_c$ and thickness $D = 0.8\ \mu$m is located at $z = 9.2\ \mu$m, where condition (6) is satisfied. The second C_{12}^{6+} layer, with density profile exponentially decreasing from electron density $n_{e2} = 10n_c$ with scale length $L = 1\ \mu$m, is located between $10\ \mu\text{m} \leqslant z \leqslant 20\ \mu$m. The number of particles per cell for each species is 400 for the Fe layer and 36 for the C layer. An initial electron temperature of 1 keV is used to resolve the initial Debye length, and ions are initially cold.

Figure 2 shows temporal evolution for the formation of C ion shock at $t = 16$, 28, 40, and $60T$. From Fig. 2(a) one notes that C ions are preferentially accelerated by E_{internal}, and ions from the high-density side experience initially an electric field higher than those from lower density. This translates into the C velocity profile peaking in an inner area, as seen in Fig. 2(b). The peak of velocity acts as the shock predictor, as discussed in Refs. [23,24]. We refer to the moving shock field as E_{back}, and the longitudinal electric field now shows a dual-peak structure [see Fig. 2(b)]. E_{internal} decreases with time due the screening effect of the shock wave [see Figs. 2(b) and 2(c)]. Later, at a critical moment, the slope of the velocity profile tends to be locally infinite, resulting a pronounced C ion density peak there [see Fig. 2(c)]. This moment marks the breaking, or critical point of the shock. From this moment on, the fast inner ions overtake the slower outer ions, and the C velocity profile shows a multivalue, or hysteretic-like shape, as shown in Fig. 2(d). The C peak density is then reduced quickly with time, while the peak of

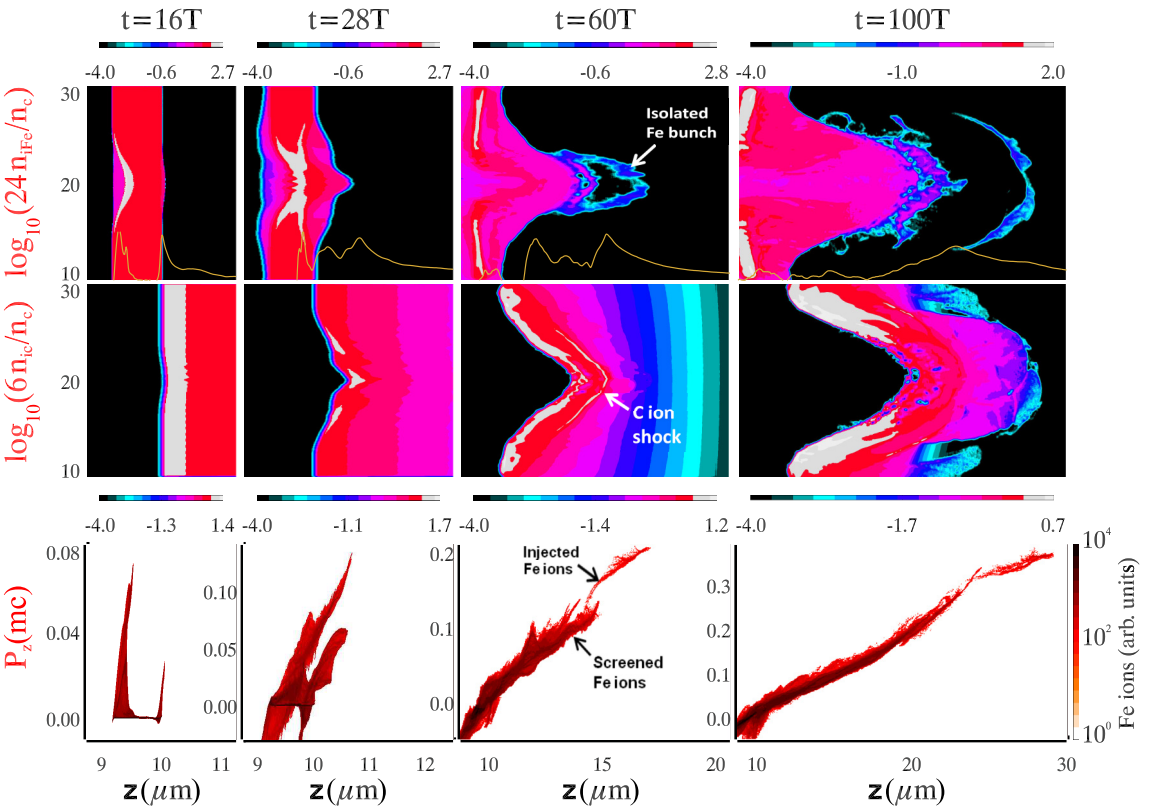

FIG. 3. (Color online) Time evolution for the three-stage Fe ion acceleration at $t = 16T$, $t = 28T$, $t = 60T$, and $t = 100T$. Top: Fe ion density $\log_{10}(24n_{iFe})$, where the solid yellow line shows the corresponding longitudinal electrostatic field E_z on the laser axis; middle: C ion density $\log_{10}(6n_{ic})$; bottom: Fe ion phase space.

E_{back} decreases slowly with time $1/\omega_{\text{pi}}t$ [24]. The velocity of the C ion shock increases almost linearly by $dv_{\text{shock}}/dt \sim 0.004c/T$, corresponding to an averaging electrostatic field of $2.34m_ec\omega/e$, which is close to the theoretical estimation above $[E_{\text{avg}} \sim (1 - e^{-1})T_h/e\lambda_D = 2.3m_ec\omega/e]$.

From Fig. 2 we can see that the rear-side Fe ions are screened by the strong C ion shock wave. If the Fe layer is thin enough, however, Fe ions from the front surface can be dominant and gain enough energy after the first two-stage acceleration. These energetic ions can then catch up with and be injected in the C ion shock for further third-stage acceleration, which is the central point of the present paper. The detailed three-stage Fe ion acceleration process is shown in Fig. 3. The left plots at $t = 16T$ correspond to the first piston-acceleration stage. Fe ions in the front surface are initially accelerated by E_{front} to maximum velocity $v_{\text{Fe},1} \sim 0.07c$. These ions arrive at rear side of the Fe layer at $t_2 = t_1 + D/v_{\text{Fe},1} \sim 20T$, and are further accelerated by E_{internal} (see $t = 28T$), which is referred to as the second sheath-acceleration stage. As the target is thin enough, Fe ions from the front surface are dominantly accelerated, and their velocity can be high enough to overrun the C ion shock at $t_3 \sim 30T$, consistent with Eq. (4). After t_3, these injected Fe ions are captured by the shock wave and further accelerated by E_{back}, separating with those screened ones. A isolated Fe ion bunch is then formed (see snapshots at $t = 60T$ and $100T$). Note that the C ion shock wave works also as a temporal lens for bunching the injected Fe ions, as the faster Fe ions in the leading part experience smaller acceleration than the lagging ions (see snapshots at $t = 60T$ and $100T$ in Fig. 3) [30]. This results in a longitudinal ultrathin ion beam (~0.3 μm corresponding to a beam duration of 1 fs) with a small energy spread as well.

The space-time evolution of the longitudinal electrostatic field E_z in Fig. 4 shows the three-stage Fe acceleration process in detail. The starting time of each acceleration stage is denoted as t_1, t_2, and t_3, respectively, in Figs. 4(a) and 4(b). The trajectories of two typical Fe^{24+} ions from the front and back

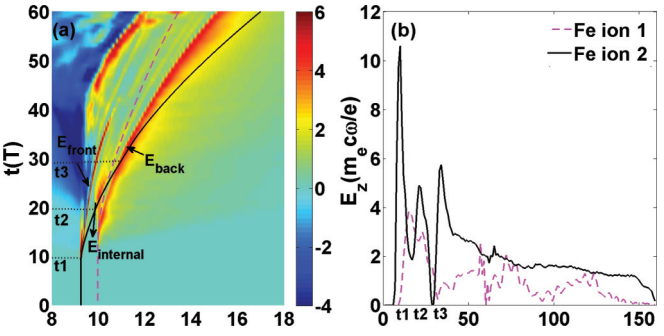

FIG. 4. (Color online) (a) The space-time evolution of the longitudinal electrostatic field E_z along the laser axis and two typical Fe^{24+} ion trajectories (black line and purple dashed line). The dashed lines are the initial boundaries of the Fe layer. (b) The longitudinal field E_z experienced by two typical accelerated Fe^{24+} ion denoted in (a).

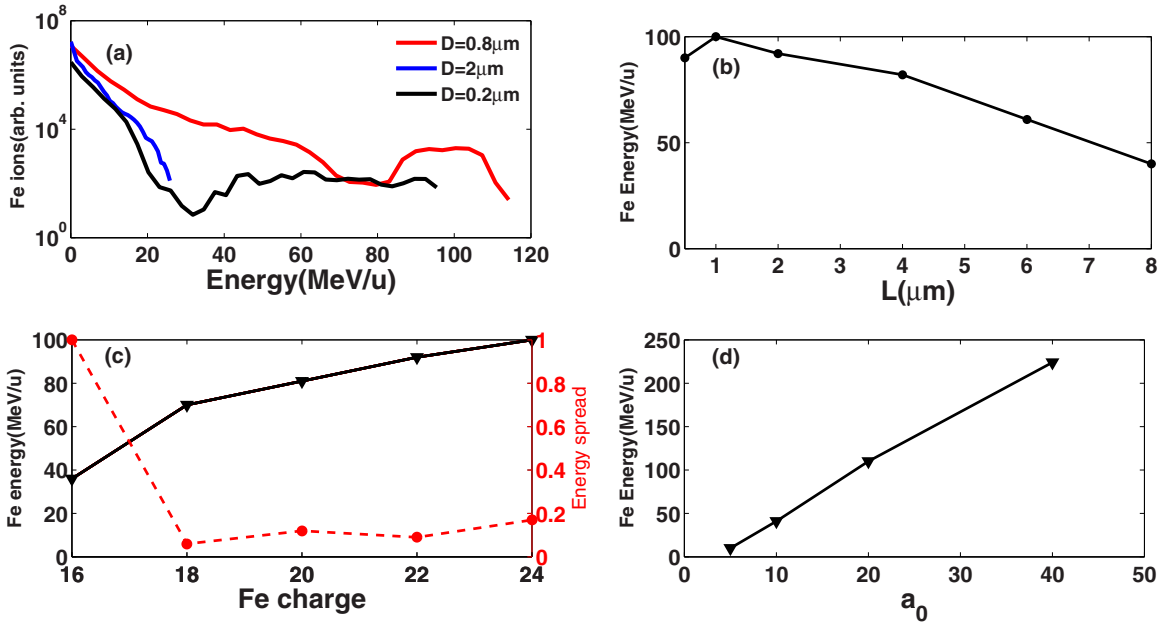

FIG. 5. (Color online) Scaling studies (scan a parameter and all other parameters are fixed) (a) Fe energy spectrum at $t = 160T$ for $D = 0.8$ μm, 2 μm, and 0.2 μm; (b) scaling the Fe energy with light ion layer scale length L; (c) scaling the Fe energy/energy spread with charge state; (d) scaling the Fe energy with the normalized vector potential a_0.

surface of the Fe layer tell the whole story. It shows that the ion from front surface (black line) is accelerated forward, passing three different electrostatic fields E_{front}, E_{internal}, and E_{back}, respectively. On the other hand, the ion from the back surface (purple dashed line) is mainly accelerated in E_{internal} and then screened by the C shock wave. Accordingly it is shown in Fig. 4(b) that the front surface ion experiences three peaks along the propagation, corresponding to the three-stage acceleration. The energy gain for the injected Fe ions at the each stage of acceleration is about 3, 7, and 90 MeV, respectively. This means that the third stage dominates in the acceleration process.

We have varied single parameters, keeping the others constant, to check the robustness and scaling of the present scheme. Figure 5(a) shows the Fe ion energy spectrum for different Fe layer thicknesses: one ($D = 0.8$ μm) satisfying condition (6) and the other two ($D = 2$ μm and $D = 0.2$ μm) not. It is found that a quasimonoenergetic Fe^{24+} beam with a well-defined peak energy of $\sim$100 MeV/u is obtained at $D = 0.8$ μm. Assuming cylindrical symmetry, the accelerated particle number in the peak area (90–110 MeV) is about 1.6×10^8. The beam duration is about 1 fs, so the produced ion current is 1.4 MA. For thicker Fe layer ($D = 2$ μm), the injection condition is not satisfied and the energy spectrum shows no pronounced peak with maximum energy of only 20 MeV. For a thinner Fe layer ($D = 0.2$ μm), the relativistically induced slab transparency plays an important role. The transmitted laser then destroys the C ion shock wave structure and prohibits the efficient third-stage acceleration. In Fig. 5(b) we can see that the Fe energy decreases with the increase of light ion layer scale length L. Figure 5(c) exhibits energy and energy spread as a function of the Fe ion charge state. It is seen that the proposed scheme is still efficient for a charge state as low as 18 but not for 16, consistent with estimation of condition (5) as $Z_1 = 56f6/12 > 28\{1 - [1 - \frac{(e-1)n_{e1}D}{5ea_0n_c}]^2\} = 16.5$. In Fig. 5(d) one observes that Fe energy is rising almost linearly with laser amplitude a_0.

Although the simulation results described so far are for the trapezoidal temporal pulse profile, such an extreme condition is actually not necessary for the scheme. For example, with the practically Gaussian shape of the laser, $a \sim a_0 \exp -[(t - 2t_0)/t_0]^2$, where $t_0 = 40T$ are taken and the other parameters are the same as in Fig. 3, our simulations verify that typical three-stage heavy ion acceleration behavior can also clearly be observed. A quasimonoenergetic Fe beam around 60 MeV with energy spread 12% is obtained in 2D simulation results. This scheme is also robust for different ion species as long as condition (6) is satisfied. Changing the target ion species from Fe^{24+} and C^{6+} to Au^{69+} and Al^{13+} shows generation of $\sim$80 MeV/u Au ion beams with a energy spread of 10%.

IV. CONCLUSIONS

In conclusion, a three-stage heavy ion acceleration scheme from compound targets by LP laser pulses is proposed. The central point of this scheme is that under proper conditions, the heavy ions preaccelerated by two-stage acceleration in the front layer surface can be energetic enough to catch up with the light ion shock wave for third-stage acceleration, without limitation from the screening effect. A criterion for this regime has been identified analytically and verified by 2D PIC simulations. It is shown that a monoenergetic Fe^{24+} beam of peak energy $\sim$100 MeV/u is produced at intensities of 1.1×10^{21} W/cm^2. The generated heavy ion bunches may be of interest for many applications that require high-energy, high-current, and quasimonoenergetic heavy ion beams.

ACKNOWLEDGMENTS

This work was supported by National Basic Research Program of China (Grant No. 2013CBA01502 and No. 2013CBA01504), the National Natural Science Foundation of China (Grant No. 11025523, No. 10935002, No. 10835003, and No. J1103206), and the National Grand Instrument Project (2012YQ030142).

[1] M. Roth *et al.*, Phys. Rev. Lett. **86**, 436 (2001); V. Yu. Bychenkov *et al.*, Plasma Phys. Rep. **27**, 1017 (2001); S. Atzeni *et al.*, Nucl. Fusion **42**, L1 (2002); M. Borghesi *et al.*, Phys. Plasmas **9**, 2214 (2002); Y. Glinec *et al.*, *ibid.* **94**, 025003 (2005).

[2] S. V. Bulanov *et al.*, Phys. Lett. A **299**, 240 (2002); T. Cowan *et al.*, Phys. Rev. Lett. **92**, 204801 (2004); L. Robson *et al.*, Nat. Phys. **3**, 58 (2007).

[3] A. J. Mackinnon, Y. Sentoku, P. K. Patel, D. W. Price, S. Hatchett, M. H. Key, C. Andersen, R. Snavely, and R. R. Freeman, Phys. Rev. Lett. **88**, 215006 (2002); S. P. Hatchett *et al.*, Phys. Plasmas **7**, 2076 (2000); L. Willingale *et al.*, Phys. Rev. Lett. **96**, 245002 (2006); A. Yogo *et al.*, Phys. Rev. E **77**, 016401 (2008).

[4] L. O. Silva, M. Marti, J. R. Davies, and R. A. Fonseca, C. Ren, F. S. Tsung, and W. B. Mori, Phys. Rev. Lett. **92**, 015002 (2004).

[5] D. Haberberger *et al.*, Nature Phys. **8**, 95 (2012).

[6] S. S. Bulanov *et al.*, Med. Phys. **35**, 1770 (2008); B. Eliasson *et al.*, New J. Phys. **11**, 073006 (2009); A. Macchi, S. Veghini, and F. Pegoraro, Phys. Rev. Lett. **103**, 085003 (2009); Z. M. Zhang *et al.*, Phys. Plasmas. **17**, 043110 (2010); A. Henig *et al.*, Phys. Rev. Lett. **103**, 045002 (2009); S. G. Rykovanov *et al.*, New J. Phys. **10**, 113005 (2008); C. S. Liu *et al.*, AIP Conf. Proc. **1061**, 246 (2008); A. Macchi *et al.*, Rev. Mod. Phys. **85**, 751 (2013).

[7] L. Yin *et al.*, Phys. Plasmas **14**, 056706 (2007).

[8] M. Hegelich, S. Karsch, G. Pretzler, D. Habs, K. Witte, W. Guenther, M. Allen, A. Blazevic, J. Fuchs, J. C. Gauthier, M. Geissel, P. Audebert, T. Cowan, and M. Roth, Phys. Rev. Lett. **89**, 085002 (2002); B. M. Hegelich *et al.*, Phys. Plasmas **12**, 056314 (2005).

[9] P. McKenna, K. W. D. Ledingham, J. M. Yang, L. Robson, T. McCanny, S. Shimizu, R. J. Clarke, D. Neely, K. Spohr, R. Chapman, R. P. Singhal, K. Krushelnick, M. S. Wei, and P. A. Norreys, Phys. Rev. E. **70**, 036405 (2004); J. C. Fernández *et al.*, Laser Part. Beams **23**, 267 (2005).

[10] B. M. Hegelich *et al.*, Nature (London) **439**, 441 (2006).

[11] A. V. Korzhimanov, E. S. Efimenko, S. V. Golubev, and A. V. Kim, Phys. Rev. Let. **109**, 245008 (2012).

[12] D. Habs *et al.*, Prog. Part. Nucl. Phys. **46**, 375 (2001).

[13] D. G. Koshkarev, Laser Part. Beams **20**, 595 (2002).

[14] D. Schardt *et al.*, Rev. Mod. Phys. **82**, 383 (2010).

[15] N. A. Tahir *et al.*, Phys. Rev. Lett. **95**, 035001 (2005).

[16] G. Agakishiev *et al.*, Phys. Rev. Lett. **108**, 072301 (2012).

[17] H. Schwoerer *et al.*, Nature (London) **439**, 445 (2006); T. Zh. Esirkepov *et al.*, Phys. Rev. Lett. **89**, 175003 (2002).

[18] N. Milosevic, V. P. Krainov, and T. Brabec, Phys. Rev. Lett. **89**, 193001 (2002); H. G. Hetzheim and C. H. Keitel, *ibid.*, **102**, 083003 (2009).

[19] S. Kahaly, S. Monchocé, H. Vincenti, T. Dzelzainis, B. Dromey, M. Zepf, Ph. Martin, and F. Quéré, Phys. Rev. Lett. **110**, 175001 (2013).

[20] T. Esirkepov, M. Borghesi, S. V. Bulanov, G. Mourou, and T. Tajima, Phys. Rev. Lett. **92**, 175003 (2004).

[21] A. P. L. Robinson *et al.*, New J. Phys. **10**, 013021 (2008).

[22] P. Mora, Phys. Rev. Lett. **90**, 185002 (2003).

[23] A. E. Kaplan, B. Y. Dubetsky, and P. L. Shkolnikov, Phys. Rev. Lett. **91**, 143401 (2003).

[24] T. Grismayer and P. Mora, Phys. Plasmas **13**, 032103 (2006).

[25] J. Fuchs *et al.*, Phys. Rev. Lett. **99**, 015002 (2007).

[26] J. Fuchs *et al.*, Nature Phys. **2**, 48 (2006).

[27] F. Fiuza, A. Stockem, E. Boella, R. A. Fonseca, L. O. Silva, D. Haberberger, S. Tochitsky, C. Gong, W. B. Mori, and C. Joshi, Phys. Rev. Lett. **109**, 215001 (2012).

[28] A. A. Gonoskov, A. V. Korzhimanov, V. I. Eremin, A. V. Kim, and A. M. Sergeev, Phys. Rev. Lett. **102**, 184801 (2009).

[29] H. Y. Wang, C. Lin, Z. M. Sheng, B. Liu, S. Zhao, Z. Y. Guo, Y. R. Lu, X. T. He, J. E. Chen, and X. Q. Yan, Phys. Rev. Lett. **107**, 265002 (2011); Z. M. Sheng, K. Mima, J. Zhang, and H. Sanuki, *ibid.* **94**, 095003 (2005).

[30] X. Q. Yan, C. Lin, Z. M. Sheng, Z. Y. Guo, B. C. Liu, Y. R. Lu, J. X. Fang, and J. E. Chen , Phys. Rev. Lett. **100**, 135003 (2008).